Electrochemical Oxidation of $(Ph_4As)[IrCl_2(CO)_2]$ in the Presence of Tetra(alkyl)ammonium Salts. Electrocrystallization of Different Forms of Iridium-Based Linear Chain Complexes

Monika Wysocka,[†] Krzysztof Winkler,*[,†] Jay R. Stork,[‡] and Alan L. Balch*[,‡]

Institute of Chemistry, University of Bialystok, 15-399 Bialystok, Poland, and Department of Chemistry, University of California, Davis, California 95616

Received October 17, 2003. Revised Manuscript Received December 10, 2003

The conducting iridium complexes $(TAA)_x[IrCl_2(CO)_2]$ (where TAA is tetra(*n*-hexyl)-ammonium, tetra(*n*-butyl)ammonium, and tetra(ethyl)ammonium cation, and $x = 0.55$, 0.62, and 0.55, respectively) were electrochemically synthesized on a gold electrode through electro-oxidation of $[IrCl_2(CO)_2]^-$ in various organic solvents (dichloromethane, 1,2-dichloroethane, acetonitrile, and 4:1 toluene/acetonitrile) using cyclic voltammetry. In dichloromethane and 1,2-dichloroethane electrocrystallization results in formation of long, randomly distributed crystalline needles on the electrode surface. The solid phase grows by a progressive nucleation mechanism followed by one-dimensional growth of microcrystals. These crystals are reversibly reduced in a subsequent anodic voltammetric potential scan. They can also be oxidized at more positive potentials. This second oxidation process results in structural changes of the solid phase and its slow dissolution. In a solution containing tetra(*n*-butyl)ammonium cations, the deposit forms two distinct structures that can be observed visually. The initially produced film forms an irregular porous structure on the electrode surface. Subsequently, needlelike crystals are deposited on the electrode surface. In a toluene/acetone mixture the process of $[IrCl_2(CO)_2]^-$ oxidation under multicyclic voltammetry conditions results in the formation of a stable electroactive species on the electrode surface. In polar solvents, such as *N*,*N*-dimethylformamide or dimethyl sulfoxide, the irreversible oxidation of $[IrCl_2(CO)_2]^-$ occurs without precipitation of any deposit at the electrode surface.

Introduction

Recently, there has been renewed interest in the preparation and properties of compounds that contain one-dimensional chains of metal centers.[1−5] The largest class of 1-D inorganic compounds are square-planar d^8 complexes that form columnar stacks in the solid state.[3,4] In these structures metal−metal bonds are formed by the overlap of their d_{z^2} and p_z orbitals.[6] Oxidative doping of such 1-D inorganic compounds can produce a mixed-valence state that leads to the formation of conductive materials.[5] The unusual properties of these materials make them very attractive for nanotechnology as they offer the possibility of developing electronic devices with very small dimensions.[7−10]

Dihalodicarbonyliridate(I) complexes show a tendency to form linear chains through metal−metal interaction in solid state.[11] These compounds were prepared by treating K_2IrX_6 (where X is a halogen anion) with carbon monoxide under pressure[12,13] or heating in formic acid solution.[14] Krogmann and Geserich presented the first direct structural evidence for the presence of linear chains of $Ir(CO)_2Cl_2^{0.6-}$ units through single-crystal and powder diffraction methods.[15] The negative charge on the iridium complex ions is compensated by alkali metal counterions. The stoichiometry of these solid crystals depends only slightly on the cation involved. Therefore, the iridium center in the anionic complex has a frac-

* Authors to whom correspondence should be addressed. E-mail: albalch@ucdavis.edu or winkler@cksr.ac.bialystok.pl.
[†] University of Bialystok.
[‡] University of California.

(1) Bera, J. K.; Dunbar, K. R. *Angew. Chem., Int. Ed.* **2002**, *41*, 4453.
(2) Caseri, W. R.; Chanzy, H. D.; Feldman, K.; Fontana, M.; Smith, P.; Tervoort, T. A.; Goossens, J. G. P.; Meijer, E. W.; Schenning, A. P. H. J.; Dolbyna, I. P.; Debije, M. G.; de Haas, M. P.; Warman, J. M.; van de Craats, A. M.; Friend, R. H.; Sirringhaus, H.; Stutzmann, N. *Adv. Mater.* **2003**, *15*, 125.
(3) Vickery, J. C.; Olmstead, M. M.; Fung, E. Y.; Balch, A. L. *Angew. Chem., Int. Ed.* **1997**, *36*, 1179.
(4) *Extended Linear Chain Compounds, Vols. 1−3*; Miller, J. S., Ed.; Plenum: New York, 1982.
(5) Williams, J. M.; Schultz, A. In *Molecular Metals;* Hatfield, W. E., Ed.; Plenum: New York, 1979; p 337.
(6) Miller, J. S.; Epstein, A. J.In *Progress in Inorganic Chemistry;* Lippard, S. J., Ed.; Wiley: New York, 1976; Chapter 1.
(7) *Molecular Semiconductors*; Lehn, J. M., Rees, C. W., Eds.; Springer-Verlag: New York, 1982.
(8) *Molecular Electronic Devices*; Carter, F., Ed.; Marcel Dekker: New York, 1982.
(9) Simon, J.; Andre, J.-J.; Skoulios, A. *J. Nouv. Chim.* **1986**, *10*, 295.
(10) Simon, J.; Tournilhac, F.; Skoulios, A. *J. Nouv. Chim.* **1986**, *11*, 383.
(11) Reis, A. H., Jr. In *Extended Linear Chain Compounds. Vol.1*; Miller, J. S., Ed.; Plenum: New York, 1982; Chapter 5.
(12) Malatesta, L.; Angoletta, M. *J. Inorg. Nucl. Chem.* **1958**, *8*, 273.
(13) Malatesta, L.; Canjiani, F. *J. Inorg. Nucl. Chem.* **1961**, *19*, 81.
(14) Cleare, M. J.; Griffith, W. P. *J. Chem. Soc. A* **1970**, 2788.
(15) Krogmann, K.; Geserich, H. P. In *Extended Interactions Between Metal Ions In Transition Metal Complexes*; Interante, L. V., Ed.; American Chemical Society: Washington DC, 1974.

10.1021/cm035029r CCC: $27.50
Published on Web 01/31/2004

tional oxidation state in the range of +1.39 to +1.44.[16,17] These materials exhibit a metallic copper luster in reflected light and metallic-like conductivity in the range 0.1 to 5 Ω^{-1} cm^{-1}.[16,17] This high conductivity is attributed to electron delocalization in a band of partially filled, overlapping iridium d_{z^2} orbitals.

An increasingly popular method for the preparation of low-dimensional molecular solids involves crystallization of these materials under electrochemical conditions.[18−20] Oxidation of an electron-donor molecule in the presence of anions or reduction of an electron-acceptor in the presence of cations results in crystal growth on the electrode surface. Crystals of high quality can be obtained in this fashion, and the process of crystal growth may be controlled by means of exterior physical conditions such as applied potential, current density, solvent, and supporting electrolyte. Much of the focus in prior work in the area of electro-crystallization has involved the synthetic aspects of the technique.[21] Less attention has been given to the electrochemistry involved in the deposition and subsequent manipulation of the materials themselves.

Electro-crystallization has been successfully employed for numerous 1-D crystals of transition metal complexes with interesting electronic properties. Alcacer and Maki reported formation of metal dithiolate−perylene complexes with the formula $[Pe]_2[MS_4C_4(CN)_4]$ (M = Ni, Cu, Pd) under electrochemical conditions.[22] Highly conducting Krogmann's salts $K_2Pt(CN)_4X_{0.3}\cdot 3H_2O$ (X = Cl, Br) were electrochemically prepared.[23,24] In this case, the product of $[Pt(CN)_4]^{2-}$ oxidation forms long needles on the electrode surface. Similar behavior has been reported for the process of $[Pt(C_2O_4)_2]^{2-}$ electro-oxidation.[25] Electrochemical procedures for preparation of one-dimensional Magnus' green salts $Pt(NH_3)_4\cdot PtCl_4$ and $Pt(NH_3)_4\cdot PtCl_6$,[26] and mixed valence platinum complexes $[Pt(en)_2][PtCl_2(en)_2](ClO_4)_4$,[27] have been reported. In the latter, platinum ions are connected through halogen bridges to form one-dimensional chains. A mixed-valence 1-D compound of rhodium, $[Rh(MeCN)_4](BF_4)_{1.5}$, has been electro-synthesized from a dinuclear precursor, $[Rh(MeCN)_4]_2^{3+}$.[28] Electro-crystallization of metal−tetracyanoquinodimethane[29] and metal−phthalocyanine[30−32] complexes has also been extensively investigated. The syntheses of several organometallic−teracyanoquinodimethane charge-transfer complexes, including $[(C_5Me_5)_2Fe]_2[TCNQ]_2$,[33] $[(C_6Me_6)_2M]_2[X]_2$ (M = Fe, Ru and X = tetracyanoquinodimethane, tetrafluorotetracyano-quinodimethane, *o*-dichlorotetracyanoquinodimethane),[34,35] and $[(C_5Me_5)Ru$-$(2_2$-1,4-cyclophane)-$Ru(C_5Me_5)][TCNQ]_2$,[36] were accomplished by electrocrystallization. All these materials are formed on the working electrode upon reduction of the acceptor species in the presence of organometallic cations.

Here we report the electrochemical synthesis of new materials obtained by electrochemical oxidation of tetraphenylarsonium dichlorodicarbonyliridate(I), $(Ph_4As)[IrCl_2(CO)_2]$ and demonstrate that three distinctly different materials can be obtained from this one precursor depending upon the conditions used for the electrooxidation.

Experimental Section

Materials. Tetraphenylarsonium dichlorodicarbonyliridate(I), $(Ph_4As)[IrCl_2(CO)_2]$, was synthesized according to the method described in the literature.[37] The supporting electrolytes: tetra(ethyl)ammonium perchlorate (Fluka), tetra(*n*-butyl)ammonium perchlorate (Sigma Chemical Co.), tetra(*n*-hexyl)ammonium perchlorate (Fluka), tetra(ethyl)ammonium tetrafluoroborate (Sigma), and tetra(ethyl)ammonium hexafluorophosphate (Fluka) were dried under vacuum for 24 h prior to use. Acetonitrile and *N*,*N*-dimethylformamide (both 99.9%, Aldrich Chemical Co.) were used as received. Toluene, dichloromethane, and 1,2-dichloroethane (Aldrich Chemical Co.) were purified by distillation over sodium under a nitrogen atmosphere.

Instrumentation. Voltammetric experiments were performed on a potentiostat/galvanostat model 283 (EG&G Instruments) or a CV-50w potentiostat (Bioanalytical Systems Inc.) with a three-electrode cell. A gold disk with a diameter of 1.5 mm (Bioanalytical Systems Inc.) was used as the working electrode. Prior to the experiment, the electrode was polished with fine carborundum paper and then with a 0.5-μm alumina slurry. Subsequently, the electrode was sonicated in water to remove the traces of alumina from the gold surface, washed with water, and dried. A silver wire immersed in 0.01 M silver perchlorate and 0.09 M tetra(*n*-butyl)ammonium perchlorate in acetonitrile and separated from the working electrode by a ceramic tip (Bioanalytical Systems Inc.) served as the reference electrode. The counter electrode was a platinum tab with an area of about 0.5 cm^2.

Simultaneous voltammetric and piezoelectric microgravimetry experiments were carried out with a home-built potentiostat and electrochemical quartz crystal microbalance, EQCM 5510, of the Institute of Physical Chemistry (Warsaw, Poland). Because plano-convex quartz crystals confine acoustic energy to the center of the crystal much better than the plano-plano crystals,[38] the former were used. The 14-mm diameter, AT-cut, plano-convex quartz crystals with 5 MHz resonance frequencies were obtained from Omig (Warsaw, Poland). A 100-nm thick gold film, which was vacuum deposited on the

(16) Buravov, L. N.; Stepanova, R. N.; Khidekel, M. L.; Shchegolev, I. F. *Dokl. Akad. Nauk SSSR*, **1972**, *203*, 819.
(17) Ginsberg, A. P.; Koepke, J. W.; Hauser, J. J.; West, K. W.; DiSalvo, F. J.; Sprinkle, C. R.; Cohen, R. L. *Inorg. Chem.* **1976**, *15*, 514.
(18) Ward, M. D. In *Electroanalytical Chemistry, Vol. 16*; Bard, A. J., Ed.; Marcel Dekker: New York, 1989; Chapter 3.
(19) Ward, M. D. In *SupramolecularArchitecture: Synthetic Control In Thin Films And Solids*; Bein, T., Ed.; Americal Chemical Society: Washington DC, 1992; Chapter 17.
(20) Awano, H.; Sakai, S.; Kuriyama, T.; Ohba, Y. *Bull. Chem. Soc. Jpn.* **1994**, *67*, 1737.
(21) Batail, P.; Boubekeyr, K.; Fourmigué, M.; Gabriel, J.-C. *Chem. Mater.* **1998**, *10*, 3005.
(22) Alcacer, L.; Maki, A. H. *J. Phys. Chem.* **1974**, *78*, 215.
(23) Miller, J. S. *Science* **1976**, *194*, 189.
(24) Williams, J. M.; Gerrity, D. P.; Schultz, A. J. *J. Am. Chem. Soc.* **1977**, *99*, 1668.
(25) Xu, L.; Dong, S. *Electrochim. Acta* **1994**, *39*, 2599.
(26) Awano, H.; Kumazawa, T.; Kasuya, K. *Electrochim. Acta* **1997**, *42*, 483.
(27) Pei, J.; Li, X. *J. Solid State Electrochem.* **2000**, *4*, 131.
(28) Finniss, G. M.; Canadell, E.; Campana, C.; Dunbar, K. R. *Angew. Chem., Int. Ed. Engl.* **1996**, *35*, 2772.
(29) Kathirgamanathan, P.; Rosseinsky, D. R. *J. Chem. Soc. Chem. Commun.* **1980**, 839.
(30) Ward, M. D. *Inorg. Chem.* **1986**, *25*, 4444.
(31) Orihashi, Y.; Kobayashi, N.; Tsuchida, E.; Matsuda, H.; Nakanishi, H.; Kato, M. *Chem. Lett.* **1985**, 1617.
(32) Tsuchida, E.; Orihashi, Y.; Kobayashi, N.; Ohno, H. *Synth. Met.* **1986**, *15*, 201.
(33) Orihashi, Y.; Ohno, H.; Tsuchida, E.; Matsuda, H.; Nakanishi, H.; Kato, M. *Chem. Lett.* **1987**, 601.
(34) Ward, M. D.; Johnson, D. C. *Inorg. Chem.* **1987**, *26*, 4213.
(35) Miller, J. S.; Calabrese, J. C.; Epstein, A. J.; Bigelow, R. W.; Zhang, J. H.; Reiff, W. M. *J. Chem. Soc. Chem. Commun.* **1986**, 1026.
(36) Ward, M. D.; Fagan, P. J.; Calabrese, J. C.; Johnson, D. C. *J. Am. Chem. Soc.* **1989**, *111*, 1719.
(37) Forster, D. *Inorg. Nucl. Chem. Lett.* **1969**, *5*, 433.
(38) Hiller, A. C.; Ward, M. D. *Anal. Chem.* **1992**, *64*, 2539.

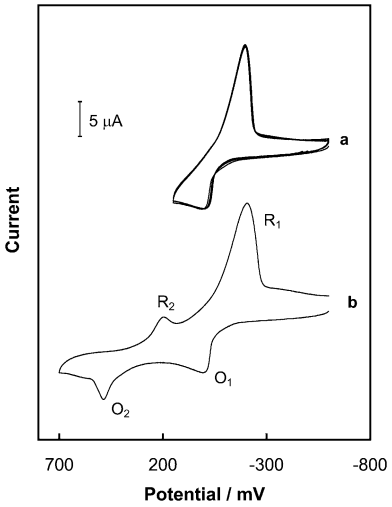

Figure 1. Cyclic voltammograms recorded in dichloromethane containing 1.75 mmol dm^{-3} $(Ph_4As)[IrCl_2(CO)_2]$ and 0.06 mol dm^{-3} tetra(ethyl)ammonium perchlorate at a gold electrode (1.5 mm diameter). (a) Multicyclic (5) scans from −600 to +180 mV. (b) A single scan from −600 to +700 mV. The sweep rate was 100 mV s^{-1}.

quartz crystal, served as the working electrode. The projected region of this Au electrode was 5 mm in diameter. The area of the circuit center spot and two contacting radial strips was 0.24 cm^2. Unpolished quartz crystals were used for better adherence of the film. The sensitivity of the mass measurement calculated from the Saurbrey equation was 17.7 ng Hz^{-1} cm^{-2}.

FT-IR spectra were recorded using a Magna IR 550 Series II Spectrometer. A spectral resolution of 4 cm^{-1} was used. All samples were in the form of a KBr pellet.

Scanning electron micrograph (SEM) images were obtained with the use of a LEO 435 vp microscope. The acceleration voltage of the electron beam was 7 kV. Films for SEM studies were prepared by constant potential electrodeposition at a gold foil. The film-covered electrode was rinsed with the solvent used for electrodeposition and then placed under the microscope.

Results and Discussion

Electrochemical Behavior of $[IrCl_2(CO)_2]^-$ in Dichloromethane Containing $(Et_4N)(ClO_4)$. The process of $[IrCl_2(CO)_2]^-$ electro-oxidation was studied in a variety of solvents containing different supporting electrolytes. However, dichloromethane containing tetra(ethyl)ammonium perchlorate was used most extensively in these studies. Results obtained in this system were used as a reference for other solvents and supporting electrolytes.

Typical voltammograms recorded in a dichloromethane solution containing $(Ph_4As)[IrCl_2(CO)_2]$ and TEAP as a supporting electrolyte are shown in Figure 1. No reduction current is observed in the negative potential range. At potentials more positive than −100 mV, oxidation of the iridium complex occurs (peak O_1) as seen in Trace a. As shown in Trace b of Figure 1, at more positive potentials, additional oxidation, O_2, and reduction, R_2, peaks are observed in the voltammogram. The charge corresponding to the R_2 peak is significantly lower than the charge of the O_2 peak.

These oxidation processes result in the formation of a crystalline solid phase on the electrode surface. The morphology of the deposit formed at potentials of peak O_1 at the surface of a gold electrode is shown in Figure 2. For short deposition times, randomly oriented long thin needles 12 μm long and 0.25 μm thick are formed on the electrode surface (Figure 2a). Upon lengthier electro-crystallization, long, randomly oriented crystal-

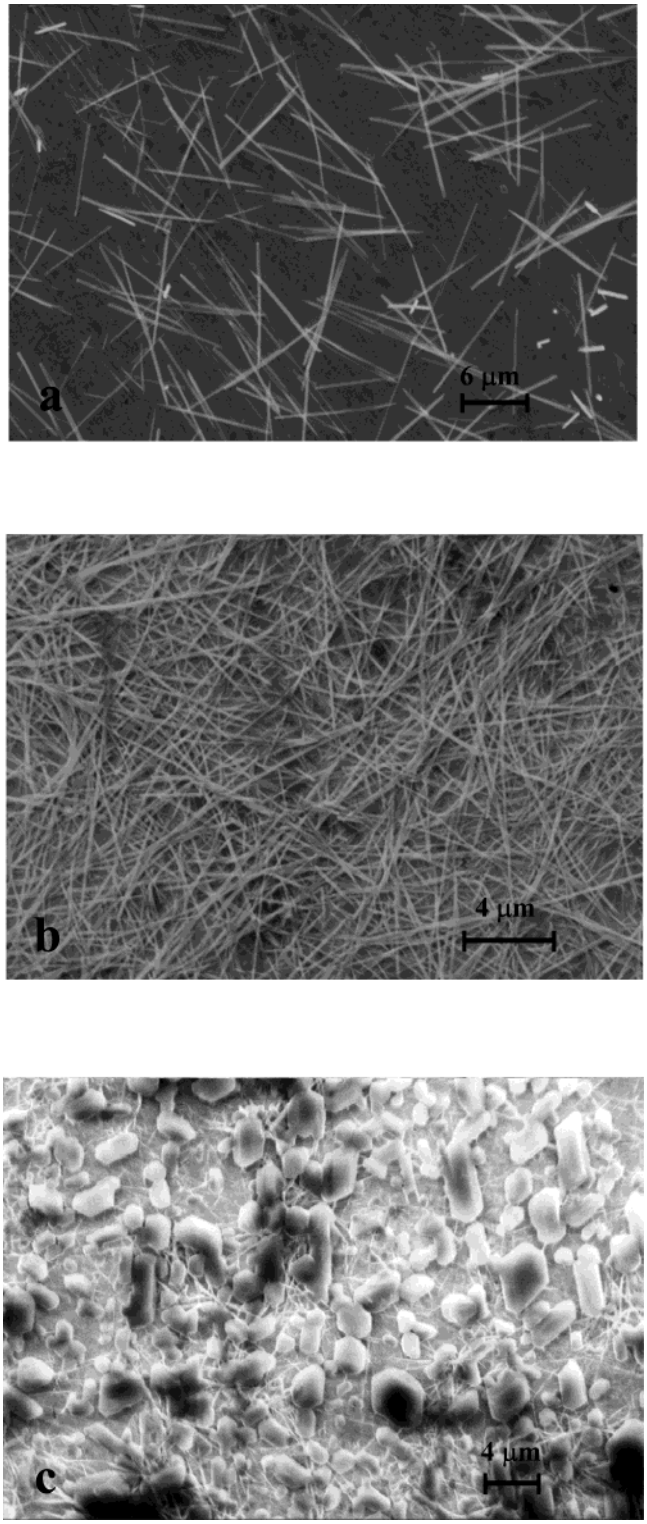

Figure 2. (a) SEM images of the electrochemically oxidized deposit on a gold-evaporated-on-mica electrode in dichloromethane solution containing 2.00 mmol dm^{-3} $(Ph_4As)[IrCl_2(CO)_2]$ and 0.06 mol dm^{-3} tetra(ethyl)ammonium perchlorate. (a) The deposit produced at a constant potential of 200 mV for 30 s. (b) The deposit produced at +200 mV for 180 s. (c) SEM images of the deposit after oxidation at +600 mV for 120 s. To obtain this image the dispersed particles were collected and placed on gold foil before the SEM image was prepared.

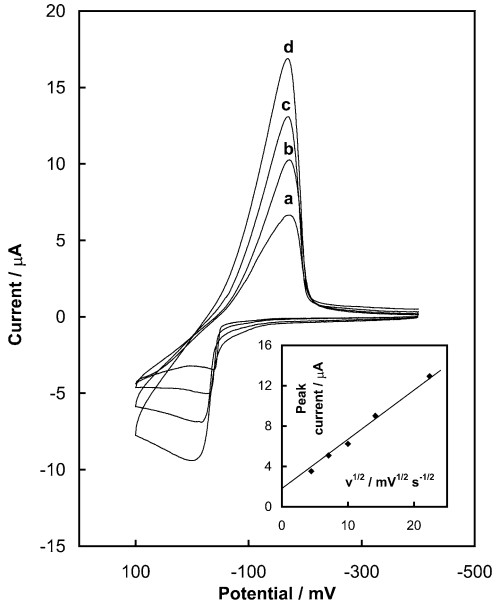

Figure 3. Cyclic voltammograms recorded in dichloromethane containing 1.80 mmol dm^{-3} $(Ph_4As)[IrCl_2(CO)_2]$ and 0.06 mol dm^{-3} tetra(ethyl)ammonium perchlorate at a gold electrode (1.5 mm diameter). The sweep rates were (a) 20, (b) 50, (c) 100, and (d) 200 mV s^{-1}. The inset shows a plot of the anodic peak current vs the square root of sweep rate.

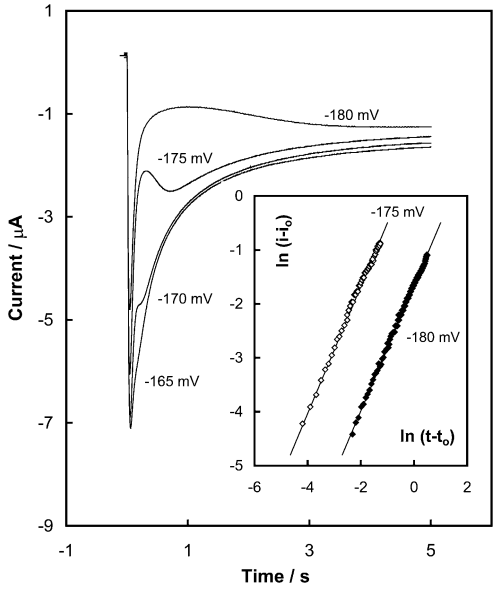

Figure 4. Chronoamperometric curves of the oxidation recorded in dichloromethane containing 1.80 mmol dm^{-3} $(Ph_4As)[IrCl_2(CO)_2]$ and 0.06 mol dm^{-3} tetra(ethyl)ammonium perchlorate at a gold electrode (1.5 mm diameter). Oxidation potentials are indicated on the figure. The inset shows a logarithmic analysis of the rising part of $i-t$ transients obtained for −180 and −175 mV.

lites appear on the electrode surface as seen in Figure 2b. The deposit formed at potentials of the O_1 peak is completely reduced in the cathodic cycle at potentials of peak R_1. SEM and AFM examination of the electrode surface after constant potential oxidation at −100 mV followed by reduction of the deposit at −400 mV show the absence of any deposit on the electrode surface.

Cyclic voltammograms were recorded at different scan rates, from 20 to 500 mV/s, as shown in Figure 3. The anodic peak current was proportional to the square root of sweep rate, $v^{1/2}$, (inset in Figure 3) with a positive intercept on the current axis. Such features are commonly observed for a deposition reaction that is controlled by nucleation.[39] The growth of this phase on the electrode surface was also probed by chronoamperometry. Anodic current−time ($i-t$) transients recorded during the first 5 s of the potential step are shown in Figure 4. The potential was stepped from −500 mV to various potentials in the range of the onset of the oxidation peak O_1. The initial decay of the oxidation current is followed by a rising transient. After reaching a maximum value, the current subsequently decreases slowly with time. The shape of the chronoamperometric curves clearly indicates that the process of $[IrCl_2(CO)_2]^-$ electro-oxidation involves the phenomena of nucleation and subsequent growth. To determine the nucleation and growth kinetics, the rising parts of the chronoamperometric curves were analyzed in the terms of following equation:

$$i - i_o = K(t - t_o)^n \qquad (1)$$

Values of the exponent n and the constant K depend on the type of nucleation (instantaneous or progressive) and on the type of growth (1, 2, or 3-dimensional).[40−43] The double logarithmic analysis produced excellent straight lines with a slope of 1.14 ± 0.06 as shown in the inset in Figure 4. A linear ln i − ln t relationship with a slope equal to unity is predicted for progressive nucleation followed by one-dimensional growth of needle-like microcrystals. In this case, the $i-t$ relationship is expressed as follows:[44]

$$i - i_o = nFAL^2k(t - t_o) \qquad (2)$$

where A is the nucleation rate constant, k is the rate constant for the crystal growth, and L is the length of nuclei.

Figure 5 shows the electrochemical behavior of the film formed under chronoamperometric conditions at 0 V upon cathodic (a) and anodic (b) potential sweeps. For the same deposition times the ratio of the charge of the oxidation peak, Q_{O2}, to the charge of the reduction process, Q_{R1}, is constant at 0.65.

Films formed on the electrode surface at different potentials were also studied by FTIR spectroscopy. The values of the relevant CO stretching frequencies are set out in Table 1. The starting material has two CO stretching vibrations at 1955 and 2042 cm^{-1}. The oxidized materials obtained by electrolysis at either +50 or +500 mV show three CO stretching vibrations at similar energies. These bands are all shifted toward higher energy relative to $[IrCl_2(CO)_2]^-$. Chemically

(39) Gunawardena, G.; Hills, G.; Montenegro, I. *J. Electroanal. Chem.* **1985**, *184*, 371.

(40) Abyaneh, M. Y.; Fleischman, M. *J. Electroanal. Chem.* **1981**, *119*, 197.

(41) Gunawardena, G.; Hills, G. J.; Montenegro, I.; Scharifker, J. *J. Electroanal. Chem.* **1982**, *138*, 225.

(42) Hills, G. J.; Schiffrin, D. J.; Thompson, J. *Electrochim. Acta* **1974**, *19*, 671.

(43) Harrison, J. A., Thirsk, H. R. In *Electroanalytical Chemistry Vol. 5*; Bard, A. J., Ed.; Marcel Dekker: New York, 1972; Chapter 2.

(44) Harrison, J. A., Thirsk, H. R. In *Electroanalytical Chemistry Vol. 5*; Bard, A. J., Ed.; Marcel Dekker: New York, 1972; Chapter 2.

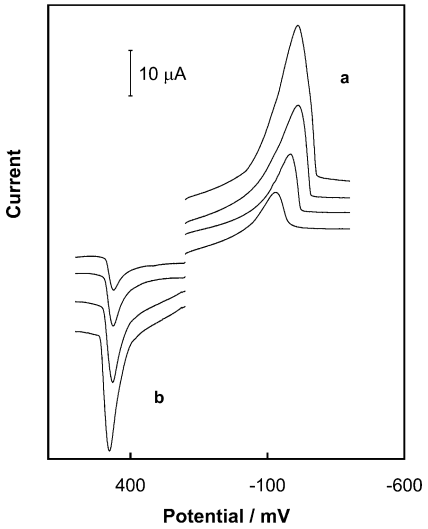

Figure 5. Voltammograms of film (a) reduction and (b) oxidation in dichloromethane solution containing 2.20 mmol dm^{-3} $(Ph_4As)[IrCl_2(CO)_2]$ and 0.06 mol dm^{-3} tetra(ethyl)-ammonium perchlorate. The film was deposited on a 1.5-mm diameter gold electrode at constant potential of 250 mV for 1, 2, 5, and 15 s.

Table 1. Infrared CO Stretching Frequencies for $(Ph_4As)[IrCl_2(CO)_2]$ and Electrochemically Prepared Compounds

compound	ν(CO) cm^{-1}	ν(CO) cm^{-1}	ν(CO) cm^{-1}
$(Ph_4As)[IrCl_2(CO)_2]$	1955	2042	
deposit formed at +50 mV	1968	2046	2071
deposit formed at +500 mV	1971	2050	2071
$K_{0.60}[IrCl_2(CO)_2]\cdot H_2O$[a]	2040	2080	2115
$(TTF)_{0.61}[IrCl_2(CO)_2]$[a]	2028	2070	

[a] Data from ref 17.

prepared $K_{0.60}[IrCl_2(CO)_2]\cdot H_2O$ also shows three CO stretching vibrations,[17] but these occur at higher energies than the CO stretching frequencies of the electrochemically prepared material.

Effect of the Supporting Electrolyte on the Electro-Oxidation of $[IrCl_2(CO)_2]^-$ in Dichloromethane. The process of $[IrCl_2(CO)_2]^-$ electro-oxidation was studied in dichloromethane containing different tetra(alkyl)ammonium salts. No effect from changing the anion in the supporting electrolyte has been observed. Voltammograms of the electro-oxidation of $[IrCl_2(CO)_2]^-$ recorded in the presence of tetra(ethyl)-ammonium perchlorate, tetrafluoroborate, or hexafluorophosphate are the same. However, the cation in the supporting electrolyte has a very significant influence on the process of $[IrCl_2(CO)_2]^-$ electro-oxidation. Figure 6 shows cyclic voltammmograms obtained in dichloromethane containing tetra(ethyl)ammonium perchlorate, tetra(*n*-butyl)ammoniumperchlorate, and tetra(*n*-hexyl)-ammonium perchlorate. The cation of the supporting electrolyte influences both the potential of the $[IrCl_2(CO)_2]^-$ oxidation and the quantity of the solid phase formed at the electrode surface. The potential of the $[IrCl_2(CO)_2]^-$ oxidations shift to a more positive value with an increase in the size of the cation in the supporting electrolyte. Additionally with tetra(*n*-butyl)-ammoniumperchlorate as supporting electrolyte there are three distinct oxidation processes, whereas with tetra(*n*-hexyl)ammonium perchlorate as the supporting

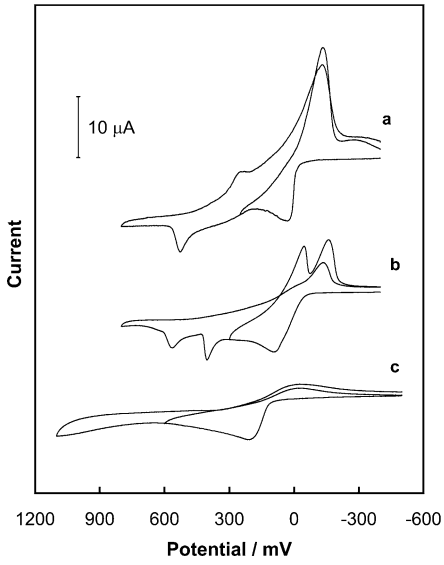

Figure 6. Cyclic voltammograms recorded in dichloromethane containing 2.45 mmol dm^{-3} $(AsPh_4)[IrCl_2(CO)_2]$ and (a) 0.06 mol dm^{-3} tetraethylammonium perchlorate, (b) 0.10 mol dm^{-3} tetra(*n*-butyl)ammonium perchlorate, and (c) 0.10 mol dm^{-3} tetra(*n*-hexyl)ammonium perchlorate at the Au (1.5 mm diameter) electrode. The sweep rate was 100 mV s^{-1}.

electrolyte there is only a hint of a second oxidative process. The yield of film formation, calculated as a ratio of charge corresponding to reduction to the oxidation charge, decreases with the increase in the size of the supporting electrolyte cation. Both effects are probably related to the differences in the solubility of the salts formed on the electrode surface. The solubility of the compound formed during electro-oxidation increases with the increase of the size of tetra(alkyl)ammonium cation. Therefore, the process of $[IrCl_2(CO)_2]^-$ oxidation can be described by the following equation:

$$[IrCl_2(CO)_2]^- + xTAA^+ \rightleftarrows (TAA)_x[IrCl_2(CO)_2] + (1 - x)\,e^- \quad (3)$$

The process of $(TAA)_x[IrCl_2(CO)_2]$ deposition and reduction of the film in the cathodic cycle was studied by the electrochemical quartz crystal microbalance technique. The relevant results are shown in Figure 7. In the positive-going scan, the current response in the potential range of the O_1 peak is associated with a change in resonance frequency of the quartz crystal due to the deposition of a solid phase on the electrode surface. The dynamics of new phase growth depend on the supporting electrolyte cation. For the initial period of film formation, the frequency decreases much faster in a dichloromethane solution containing tetra(ethyl)-ammonium perchlorate than for a solution containing tetra(*n*-butyl)ammonium perchlorate or tetra(*n*-hexyl)-ammonium perchlorate. In the negative-going scan, an increase of frequency is observed in the potential range of the R_1 reduction peak. This observation indicates that the film is removed from the electrode surface during the negative-going scan. The new phase is removed completely from the electrode surface upon reduction in a solution containing tetraethylammonium perchlorate. However, in a solution containing tetra-(*n*-hexyl)ammonium perchlorate, the limiting frequency of the negative-going scan is different from the value

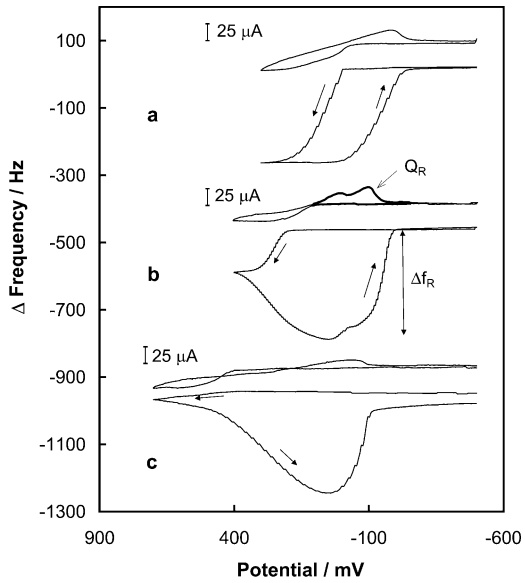

Figure 7. Voltammograms and curves of frequency change vs potential simultaneously recorded at the same Au/quartz electrode in a dichloromethane solution containing 1.80 mmol dm^{-3} $(Ph_4As)[IrCl_2(CO)_2]$ and (a) 0.06 mol dm^{-3} tetra(ethyl)-ammonium perchlorate, (b) 0.1 mol dm^{-3} tetra(*n*-butyl)ammonium perchlorate, and (c) 0.06 mol dm^{-3} tetra(*n*-hexyl)-ammonium perchlorate. The sweep rate was 20 mV s^{-1}.

of the initial frequency. This observation indicates that some of the deposit remains on the electrode surface.

Comparison of the charge of the R_1 peak, Q_{R1}, with the frequency change related to the reduction of the film, Δf_R, (Figure 7) allows the cation/anion ratio of the solid material deposited on the electrode surface to be calculated. According to the Sauerbrey equation, frequency changes, Δf_R, are correlated with the mass changes, Δm, as follows:

$$\Delta f_R = -\left[\frac{-2 \cdot f_0^{\,2}}{A \cdot (\mu\rho)^{1/2}}\right] \cdot \Delta m = K \cdot \Delta m \qquad (4)$$

where f_o is the resonance frequency of the quartz crystal, A is the piezo-electrically active area, μ is the shear modulus of the quartz, and ρ is its density.[40] According to the Faraday law, the charge consumed during reduction of the $(TAA)_x[IrCl_2(CO)_2]$ deposit, Q_R, is described by the following equation:

$$\Delta m = \frac{M}{(1-x) \cdot F} \cdot Q_{R1} \qquad (5)$$

where M is the molar weight of $(TAA)_x[IrCl_2(CO)_2]$ and F is Faraday's constant. If the coordination shell of the iridium cation is not changed during the formation of the new phase on the electrode surface, the molar mass of the deposit can be expressed as

$$M = xM_{R_4N} + M_{[Ir(CO)_2Cl_2]^-} \qquad (6)$$

It follows that eq 3 can be rewritten as

$$\Delta f_R = -K \cdot \frac{x \cdot M_{R_4N} + M_{[Ir(CO)_2Cl_2]^-}}{(1-x) \cdot F} \cdot Q_{R1} \qquad (7)$$

On the basis of the experimental values for the frequency changes, Δf_R, and charge related to the film reduction, Q_{R1}, values of x of 0.55, 0.62, and 0.55 were obtained for the deposits with tetra(ethyl)ammonium, tetra(*n*-butyl)ammonium, and tetra(*n*-hexyl)ammonium cations, respectively. These values of x are within experimental error of one another and indicate that the electrochemically prepared material is similar to the chemically prepared material reported earlier.[11−17]

Effects of the Second Electro-Oxidation on the Deposit. The two distinct oxidative processes observed voltammetrically for $[IrCl_2(CO)_2]^-$ result in clear morphological changes in the nature of the deposit. The formation of a deposit on the electrode surface during constant potential oxidation of $[IrCl_2(CO)_2]^-$ was visible to the naked eye. Photographs taken during the formation of the microcrystalline material grown from dichloromethane solution with tetra(*n*-butyl)ammonium perchlorate as the supporting electrolyte by electrolysis at +50 mV and subsequently its oxidation at +600 mV are shown in Figure 8. The initial oxidation of $[IrCl_2(CO)_2]^-$ at +50 mV results in the formation of long green needles which grow outward and perpendicular to the electrode surface as seen in part a of Figure 8. Prolonged electrolysis leads to the formation of a brush-like structure on a cylindrical electrode (Figure 8b and c). A significant increase of the oxidation current is observed when the electrode is covered with this deposit. This behavior indicates that the needlelike crystals are conductive.

The nature of this deposit changes markedly when a potential more positive than 500 mV is applied to the electrode. Oxidation under these conditions begins at the outward edges of the crystalline deposit and results in the formation of black particles at the ends of the needles as seen in Figure 8d. These particles expand outward from the electrode and can break off from the initial green needles and diffuse into the solution. Continued electrolysis of the sample results in further conversion of the green needles into the black particles. Two regions can be detected in the vicinity of the electrode: the initially formed brush-like structure and the plume of black particles as seen parts d and e of Figure 8. Finally, after an extended period of oxidation the needles are completely oxidized and only the black particles remain as seen in Figure 8f. Similar changes are seen when the deposit is formed with tetra(ethyl)-ammonium perchlorate as the supporting electrolyte, but in that case the original needles are lighter in color and the contrast between the colors of the phases is lower. The structure of the particles formed during oxidation of $[Et_4N]_{0.55}[Ir(CO)_2Cl_2]$ is shown in Figure 2c. To obtain the SEM image in this part of the figure, the particles were collected, washed, and placed on gold foil and then examined by SEM. These particles are much smaller than the particles formed during oxidation of $[n\text{-}Bu_4N]_{0.62}[Ir(CO)_2Cl_2]$

The EQCM technique was also used to study the electrochemical properties of the [tetra-(alkyl)-ammonium]$_x[IrCl_2(CO)_2]$ deposit when it undergoes the second oxidation in the very positive potential range. The results of these studies are shown in Figure 9. In dichloromethane solutions containing tetra(ethyl)ammonium perchlorate and tetra(*n*-butyl)ammonium per-

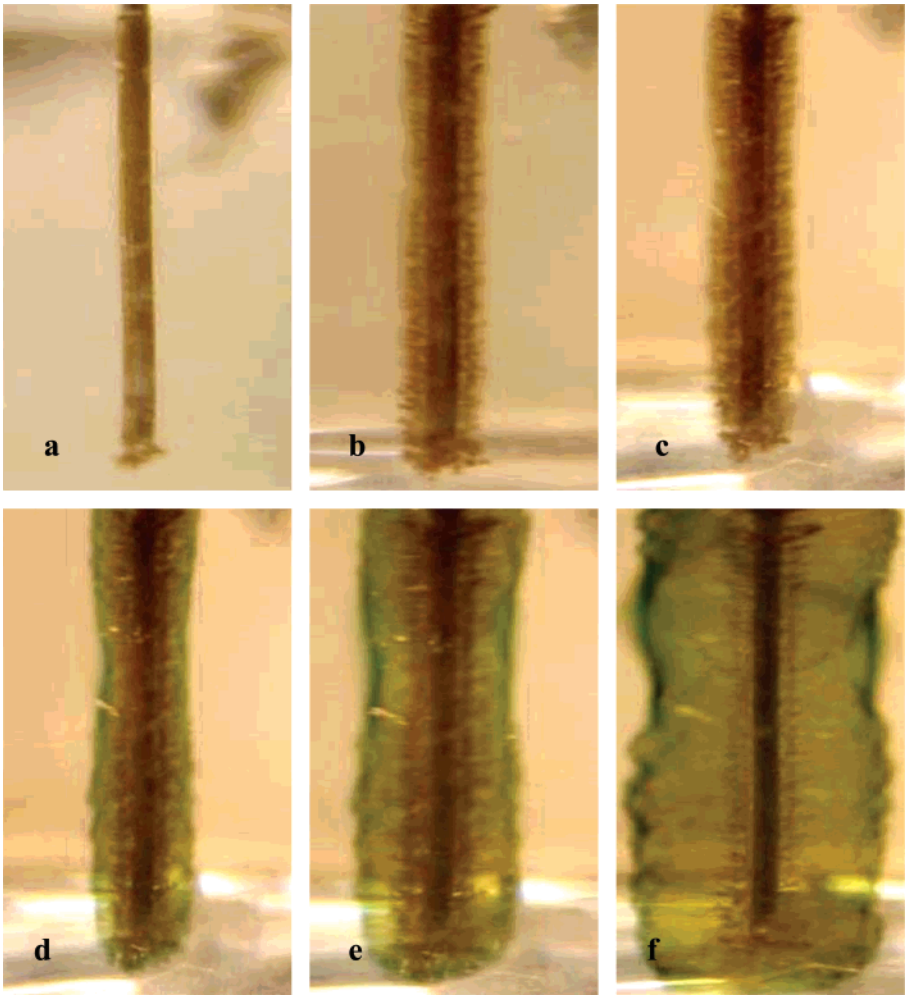

Figure 8. Photographs taken during the growth of deposit in dichloromethane containing 2.45 mmol dm^{-3} $(Ph_4As)[IrCl_2(CO)_2]$ and 0.1 mol dm^{-3} tetra(*n*-butyl)ammonium perchlorate at the platinum wire (0.2 mm diameter) with a potential of +50 mV for (a) 2, (b) 5, and (c) 15 min. Subsequently the electrode deposit was oxidized at 600 mV for (d) 4, (e) 10, and (f) 20 min.

chlorate, at positive potentials corresponding to peak O_2, the oxidation process is associated with an increase in the resonance frequency of the quartz crystal. Initially, the frequency slowly increases in the following negative-going scan. A cloud of black particles is observed in the vicinity of the electrode. In the subsequent scan, in the potential range of the O_1 peak, the frequency slightly decreases again due to the film deposition. However, the amount of film formed on the electrode is much lower than the amount of the solid-phase deposited in the initial positively going scan. Therefore, the formation of the needlelike crystals is inhibited by the new solid phase formed in the vicinity of the electrode at positive potentials.

The voltammetric response of the film formed in a solution containing tetra(*n*-butyl)ammonium perchlorate is significantly different from the electrochemical behavior of deposits produced in the presence of tetra(ethyl)ammonium and tetra(*n*-hexyl)ammonium cations. Figure 10 shows the effect of the amount of $(n\text{-}Bu_4N)_{0.62}[IrCl_2(CO)_2]$ film on its electrochemical properties upon cathodic (a) and anodic (b) scans. In both cases, two peaks, indicated as R_1' and R_1'', and O_2' and O_2'', for cathodic and anodic scans, respectively, are observed. For a short film deposition time, only peaks R_1' and O_2' are present on voltammograms. For thicker films, the charge corresponding to peaks R_1' and O_2' reaches a

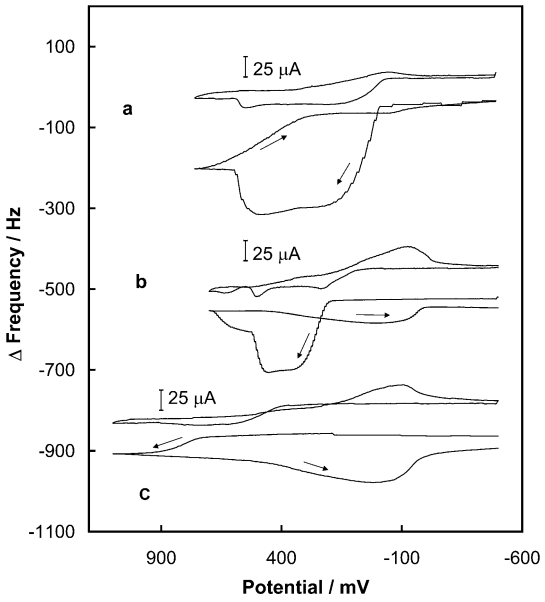

Figure 9. Voltammograms and curves of frequency change vs potential simultaneously recorded at the same Au/quartz electrode in a dichloromethane solution containing 1.80 mmol dm^{-3} $(Ph_4As)[IrCl_2(CO)_2]$ and (a) 0.06 mol dm^{-3} tetra(ethyl)-ammonium perchlorate, (b) 0.10 mol dm^{-3} tetra(*n*-butyl)-ammonium perchlorate, and (c) 0.06 mol dm^{-3} tetra(*n*-hexyl)-ammonium perchlorate. The sweep rate was 20 mV s^{-1}.

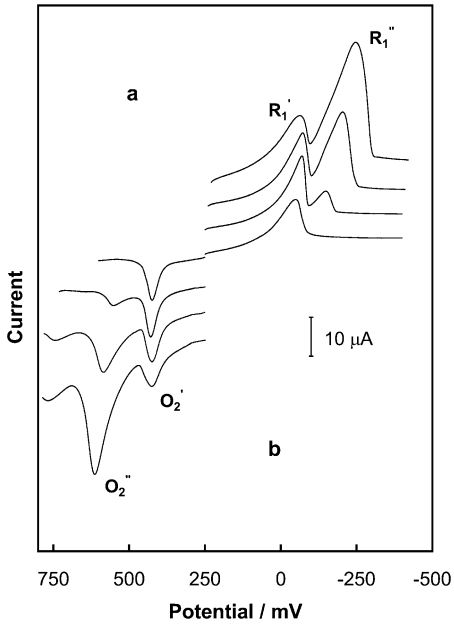

Figure 10. Voltammograms of (a) film reduction and (b) film oxidation in dichloromethane solution containing 2.20 mmol dm^{-3} $(Ph_4As)[IrCl_2(CO)_2]$ and 0.10 mol dm^{-3} tetra(*n*-butyl)-ammonium perchlorate. The film was deposited on a 1.5-mm diameter gold electrode at a constant potential of 250 mV for 1, 2, 5, and 15 s.

maximum constant value. Also, additional broad peaks R_1'' and O_2'' appear in the voltammetric curves. The limiting charge corresponding to the R_1' peak is equal to 39.8 μC cm^{-2}. The area of the $[IrCl_2(CO)_2]^-$ complex calculated on the base of crystallographic data[45] is about 3.63×10^{-15} cm^{-2}. Therefore, the monolayer coverage of the electrode by $(n\text{-}Bu_4N)_{0.62}[IrCl_2(CO)_2]$ corresponds to about 17.6 μC cm^{-2}. The maximum charge of the R_1' peak corresponds to the reduction of about 2 monolayers of $(n\text{-}Bu_4N)_{0.62}[IrCl_2(CO)_2]$.

Figure 11 shows the film morphology as a function of its thickness. The thin film (about 60 μC cm^{-2}) forms a porous structure with some needlelike outgrowths on the electrode surface (Figure 11a). Subsequently, for higher deposition charges, the formation of a dense network of fine, needlelike crystals is observed (Figure 11b). These needles are much shorter and thinner than the needles formed in dichloromethane containing tetra-(ethyl)ammonium perchlorate (See Figure 2.). In the background of Figure 11a the porous structure of the initially formed film can be seen. Finally, the surface of the electrode is covered by a hair-like film of $(n\text{-}Bu_4N)_{0.62}[IrCl_2(CO)_2]$ (Figure 11b).

At potentials more positive than about +600 mV, the oxidation of the film occurs. Dark spherical particles form during oxidation of the film. These particles slowly desorb from the electrode surface and diffuse toward the bulk of the solution. The morphology of the surface of these particles is shown in Figure 11c.

Chronoamperometric studies of $[IrCl_2(CO)_2]^-$ oxidation in dichloromethane containing tetra(*n*-butyl)ammonium perchlorate were also performed. The current decreases with time in the potential range of the O_1 peak, from −100 to +100 mV. The oxidation current depends linearly on the reciprocal of the square root of time. This behavior indicates that the rate of the electrode process is limited by the diffusion of reactants to the electrode surface. An increase of the limiting background current at long time with the increase of oxidation potential is probably related to the increase in the active area of the electrode surface due to the formation of the conducting film. The $i-t$ transients

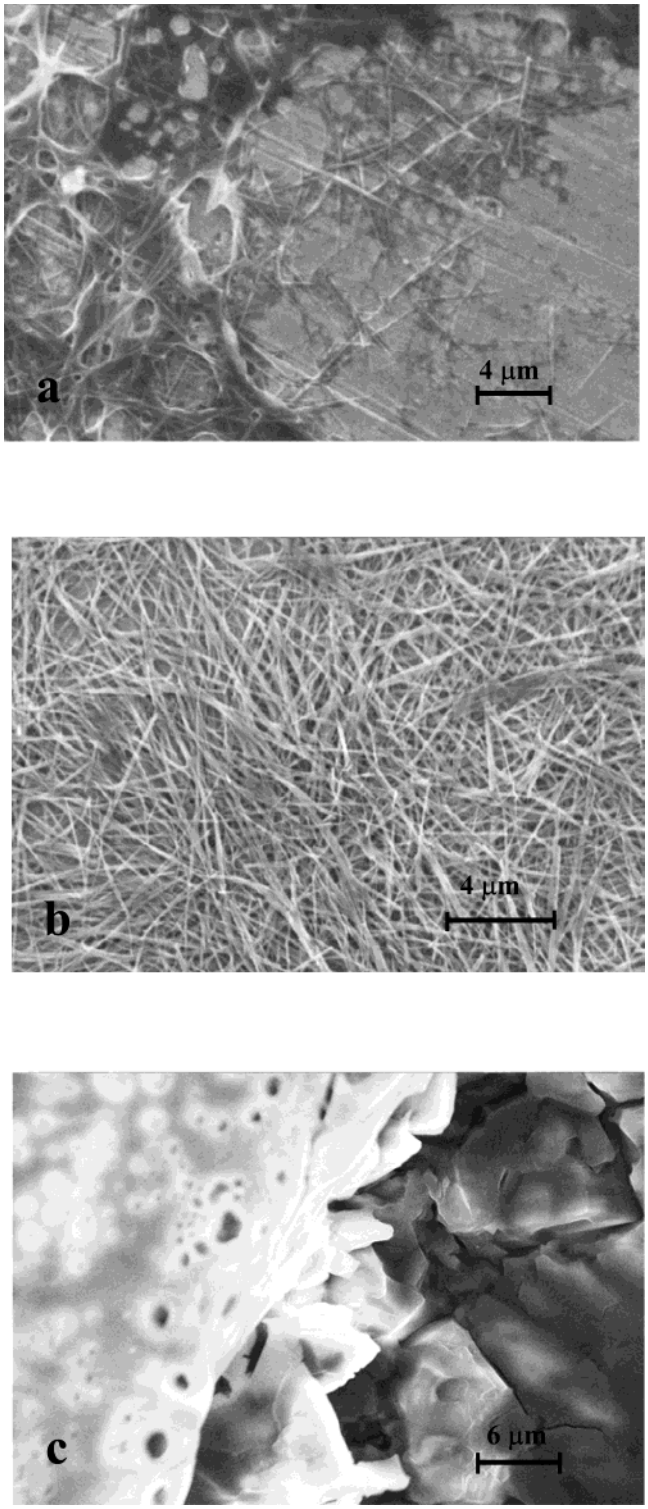

Figure 11. SEM images of the film deposited on a gold foil in dichloromethane containing 2.00 mmol dm^{-3} $(AsPh_4)[IrCl_2(CO)_2]$ and 0.1 mol dm^{-3} tetra(*n*-butyl)ammonium perchlorate. (a) The deposit produced at a constant potential of +200 mV for 15 s. (b) The deposit produced at +200 mV for 180 s. (c) The deposit after oxidation at +700 mV for 120 s.

(45) Buttry, D.; Ward, M. *Chem. Rev.* **1992**, *92*, 1355.

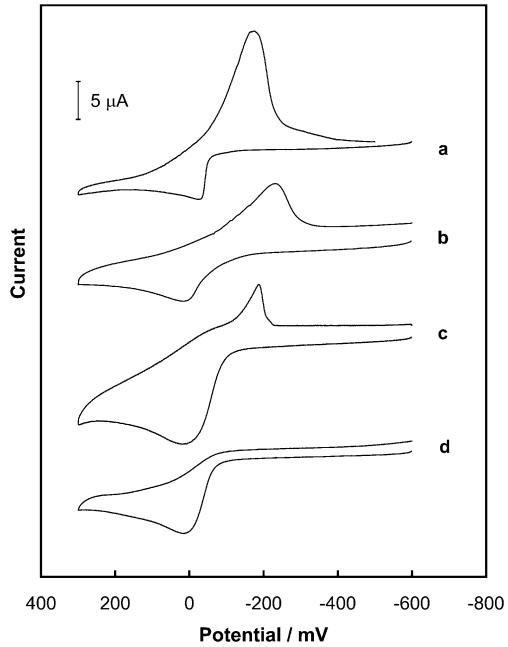

Figure 12. Cyclic voltammograms recorded in solutions of (a) dichloromethane, (b) dichloroethane (c) acetonitrile, and (d) *N*,*N*-dimethylformamide containing 1.80 mmol dm^{-3} (Ph_4As)[$IrCl_2(CO)_2$] and 0.06 mol dm^{-3} tetra(ethyl)ammonium perchlorate at a 1.5-mm diameter gold electrode. The sweep rate was 100 mV s^{-1}.

obtained upon reduction exhibit a shape that is indicative of reduction of the solid phase from the electrode surface. When the solid phase is completely removed from the electrode surface, the current suddenly drops to its background value.

Solvent Effects on the Electro-Oxidation of $[IrCl_2(CO)_2]^-$. The process of $[IrCl_2(CO)_2]^-$ oxidation was investigated in various organic solvents. In Figure 12, cyclic voltammograms recorded in (a) dichloroethane, (b) dichloroethane, (c) acetonitrile, and (d) *N*,*N*-dimethylformamide are compared. In dichloromethane, 1,2-dichloroethane, and acetonitrile, the process of $[IrCl_2(CO)_2]^-$ oxidation results in deposition of material on the electrode surface. In dichloromethane, and 1,2-dichloroethane, long crystalline needles are formed on the electrode surface during $[IrCl_2(CO)_2]^-$ oxidation. In acetonitrile, an unstructured film is deposited on the electrode surface. As this deposit grows, its adherence to the surface lessens.

Particularly interesting behavior is observed for a toluene/acetonitrile (4:1, v/v) mixture. Figure 13a shows the multicyclic voltammograms in a solution containing the iridium complex and tetra(*n*-butyl)ammonium perchlorate. The steady increase in current with repeated cycling is observed that is indicative of the deposition of a redox active film. Indeed, visual observation of the electrode surface after electrolysis reveals the presence of an orange coating on the electrode. The electrode covered with this film retains its redox activity when it is transferred to a solution of toluene/acetonitrile that contains only the supporting electrolyte. However, the film is slowly removed from the surface upon repeated cycling of the potential. Relevant data are shown in trace b of Figure 13.

SEM images of the electrode surface during the deposition of film from the toluene/acetonitrile (4:1, v/v)

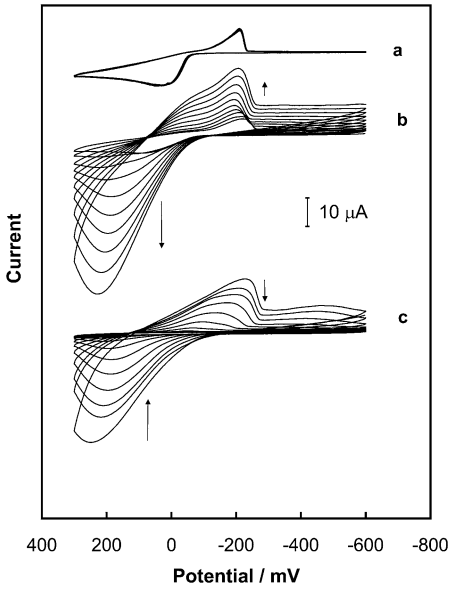

Figure 13. (a) Multicyclic voltammograms recorded in acetonitrile containing 2.25 mmol dm^{-3} (Ph_4As)[$IrCl_2(CO)_2$] and 0.10 mol dm^{-3} tetra(*n*-butyl)ammonium perchlorate at a 1.5-mm diameter gold electrode. (b) Multicyclic voltammograms recorded in toluene/acetonitrile (4:1, v:v) containing 1.90 mmol dm^{-3} (Ph_4As)[$IrCl_2(CO)_2$] and 0.10 mol dm^{-3} tetra(*n*-butyl)-ammonium perchlorate at a 1.5-mm diameter gold electrode. (c) Voltammetric response of this modified electrode after transfer to a solution of 0.10 mol dm^{-3} tetra(*n*-butyl)ammonium perchlorate in toluene/acetonitrile (4:1, v:v). The sweep rate was 100 mV s^{-1}.

mixture with tetra(*n*-butyl)ammonium perchlorate as supporting electrolyte are shown in Figure 14. After 5 deposition cycles, small island deposits appear with crystals growing outward along the electrode surface. After 10 deposition cycles the crystalline deposit covers the surface as shown in part b of Figure 14. After 25 cycles the surace reveals a coating of amorphous material along with some of the original crystallites.

In polar solvents such as *N*,*N*-dimethylformamide and dimethyl sulfoxide, the iridium complex is irreversibly electro-oxidized. In these solvents there was no evidence of the formation of a deposit on the electrode surface. A linear relation between oxidation peak current and the square root of sweep rate with intercept of zero was obtained.

Conclusions

The process of $[IrCl_2(CO)_2]^-$ electro-oxidation depends significantly on the supporting electrolyte and solvent. In dichloromethane and 1,2-dichloroethane at potentials of first oxidation step of the complex, electro-crystallization occurs which can be described by the following equation:

$$[Ir(CO)_2Cl_2]^- \underset{+(1-x)\,e^- - xTAA^+}{\overset{\text{Peak } O_1}{\underset{\text{Peak } R_1}{\rightleftharpoons}}} [Ir(CO)_2Cl_2](TAA)_x$$

$x = 0.55$ for Et_4N^+

0.62 for $n\text{-}Bu_4N^+$

0.55 for $n\text{-}Hx_4N^+$

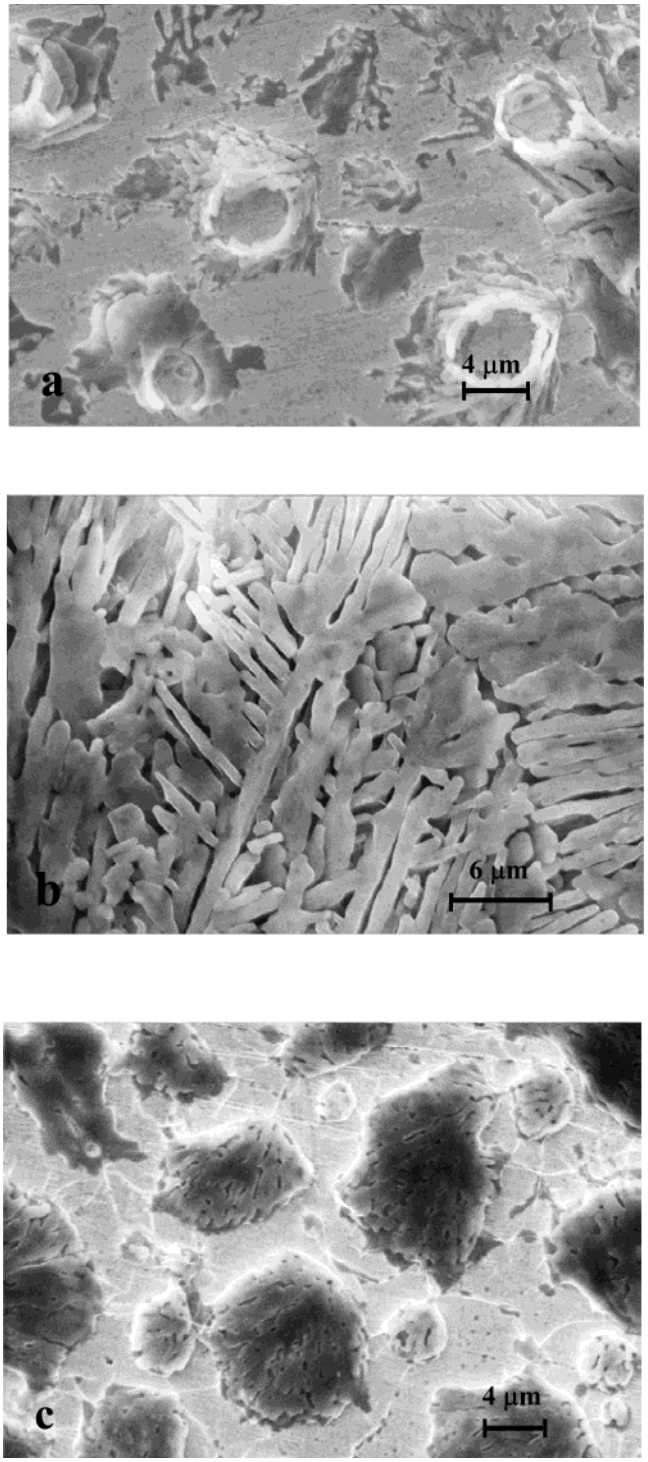

Figure 14. SEM images of the film electrodeposited on gold foil during potential cycling from −500 to +400 mV in toluene/acetonitrile (4:1, v:v) containing 2.10 mmol dm^{-3} $(AsPh_4)[IrCl_2(CO)_2]$ and 0.10 mol dm^{-3} tetra(*n*-butyl)ammonium perchlorate. Number of scans: (a) 5, (b) 10, and (c) 25. The sweep rate was 100 mV/s.

The composition of the electrochemically generated material in the potential range of the O_1 peak is very similar to that of the chemically synthesized compounds.[10−12] The deposit forms long thin needles on the electrode surface, and the increase of the current at the electrode covered with needlelike material indicates that the deposit is conductive. One-dimensional growth of the crystals indicates the anisotropy of the conductivity. It is quite likely that, similar to chemically formed compounds, the charge is transferred along the needles as a result of the overlap of iridium d_{z^2} orbitals. The negative charge on each iridium complex in the oxidized material formed in the first oxidative process is about −0.35 and this value does not vary greatly for different cations. A related study of the electrochemical formation of tetracyanoplatinum salts from aqueous solution has also examined the growth and dissolution processes for needlelike, conductive crystals.[46]

The process of deposition is strongly affected by the nature of the cation of the supporting electrolyte. The efficiency of deposition increases in order $(n\text{-}C_6H_{13})_4N^+ < (n\text{-}C_4H_9)_4N^+ < (C_2H_5)_4N^+$ due to the decrease in the solubility of the deposit formed. In dichloromethane solution containing tetra(*n*-butyl)ammonium perchlorate, two different morphologies of deposit were obtained. Initially, a rather unstructured three-dimensional deposit is formed on the electrode surface. Subsequently, fine crystalline needles are deposited. Both structures exhibit different redox properties.

At more positive potentials, the oxidation of the needlelike deposit occurs. The film changes its structure and morphology, and spherical black particles are formed at the ends of the green needles. These particles slowly desorb from the electrode surface and diffuse into the bulk of solution. This process probably results in further oxidation of the iridium complexes to forms with oxidation states higher than $Ir^{0.6}$. A number of complexes related to $[IrCl_2(CO)_2]^-$ have been prepared chemically with iridium in the Ir^2 and Ir^3 oxidation states.[12−14]

Solvent also affects the process of oxidation of $[IrCl_2(CO)_2]^-$. In strongly polar solvents the iridium complex is irreversibly electro-oxidized and no material is deposited on the electrode surface. In acetonitrile, an unstructured film is deposited on the electrode surface. Needlelike crystals are formed in dichloromethane and 1,2-dichloroethane, whereas in a toluene/acetonitrile mixture an electroactive crystalline film is deposited on the electrode surface upon potential cycling.

Acknowledgment. We thank the State Committee for Scientific Research, Poland (K.W.) and the National Science Foundation (grant CHE0070291 to A.L.B.) for financial support, D. Pham for assistance with Figure 8, and M. E. Plonska for help with the SEM images.

CM035029R

(46) Loveday, D. C.; Hillman, A. R.; Orpen, A. G.; Pringle, P. G.; Hepel, M. *J. Mater. Chem.* **1996**, *6*, 993.